BIOLOGICAL CRYSTALLOGRAPHY

ISSN 1399-0047

# The first crystal structure of a glycoside hydrolase family 17 β-1,3-glucanosyltransferase displays a unique catalytic cleft

**Zhen Qin,[a] Qiaojuan Yan,[b] Jian Lei,[a] Shaoqing Yang,[a] Zhengqiang Jiang[a]* and Shiwang Wu[a]**

[a]College of Food Science and Nutritional Engineering, Research and Innovation Center of Food Nutrition and Human Health (Beijing), China Agricultural University, Beijing 100083, People's Republic of China, and [b]Bioresource Utilization Laboratory, College of Engineering, China Agricultural University, Beijing 100083, People's Republic of China. *Correspondence e-mail: zhqjiang@cau.edu.cn

Received 18 December 2014
Accepted 7 June 2015

Edited by S. Wakatsuki, Stanford University, USA

**Keywords:** β-1,3-glucanosyltransferase; glycoside hydrolase family 17; *Rhizomucor miehei*; crystal structure; transglycosylation.

**PDB references**: *Rm*Bgt17SA, 4wtp; *Rm*Bgt17A/E189A, complex with laminaribiose, 4wtr; complex with laminaripentaose, 4wts

**Supporting information**: this article has supporting information at journals.iucr.org/d

β-1,3-Glucanosyltransferase (EC 2.4.1.–) plays an important role in the formation of branched glucans, as well as in cell-wall assembly and rearrangement in fungi and yeasts. The crystal structures of a novel glycoside hydrolase (GH) family 17 β-1,3-glucanosyltransferase from *Rhizomucor miehei* (*Rm*Bgt17A) and the complexes of its active-site mutant (E189A) with two substrates were solved at resolutions of 1.30, 2.30 and 2.27 Å, respectively. The overall structure of *Rm*Bgt17A had the characteristic $(\beta/\alpha)_8$ TIM-barrel fold. The structures of *Rm*Bgt17A and other GH family 17 members were compared: it was found that a conserved subdomain located in the region near helix α6 and part of the catalytic cleft in other GH family 17 members was absent in *Rm*Bgt17A. Instead, four amino-acid residues exposed to the surface of the enzyme (Tyr135, Tyr136, Glu158 and His172) were found in the reducing terminus of subsite +2 of *Rm*Bgt17A, hindering access to the catalytic cleft. This distinct region of *Rm*Bgt17A makes its catalytic cleft shorter than those of other reported GH family 17 enzymes. The complex structures also illustrated that *Rm*Bgt17A can only provide subsites −3 to +2. This structural evidence provides a clear explanation of the catalytic mode of *Rm*Bgt17A, in which laminaribiose is released from the reducing end of linear β-1,3-glucan and the remaining glucan is transferred to the end of another β-1,3-glucan acceptor. The first crystal structure of a GH family 17 β-1,3-glucanosyltransferase may be useful in studies of the catalytic mechanism of GH family 17 proteins, and provides a basis for further enzymatic engineering or antifungal drug screening.

## 1. Introduction

β-1,3-Glucan is a major structural component of the cell wall of fungi and yeasts. It forms a fibrillary network responsible for the mechanical strength of the cell wall (Manners *et al.*, 1973; Fontaine *et al.*, 2000). β-1,3-Glucan is also a major structural and storage polysaccharide in marine macroalgae and a constituent of plant cell walls (Fibriansah *et al.*, 2007). In fungi, β-1,3-glucan is synthesized by a plasma-membrane-bound glucan synthase complex (Mouyna *et al.*, 2013). The immature glucans are branched, cross-linked and covalently linked to other cell-wall components by structural remodelling enzyme systems, including glucanase and glucanosyltransferase, resulting in the formation of rigid three-dimensional structures (Wessels, 1988; Mouyna *et al.*, 2013).

β-1,3-Glucanosyltransferases (EC 2.4.1.–) catalyze the transfer of a glycosyl group from a β-1,3-linked glucan donor to a suitable (carbohydrate) acceptor. According to the classification of carbohydrate-active enzymes, β-1,3-glucanosyl-

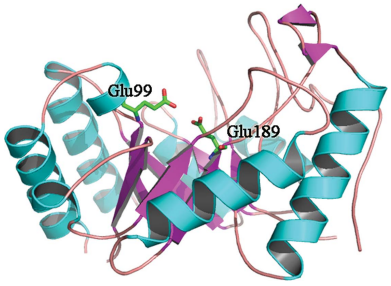

transferases are grouped into three glycoside hydrolase (GH) families: 16, 17 and 72 (CAZy; http://www.cazy.org/; Lombard *et al.*, 2014). These three different GH family $\beta$-1,3-glucanosyltransferases show cross-linking, branching and elongation functions, respectively, in the $\beta$-1,3-glucan modifying enzymes of *Aspergillus fumigatus* (Mouyna *et al.*, 2013). The three-dimensional structures of several members of GH families 16, 17 and 72 revealed a $\beta$-jelly roll, a $(\beta/\alpha)_8$ TIM-barrel and a $(\beta/\alpha)_8$ TIM-barrel, respectively (CAZy; http://www.cazy.org/; Lombard *et al.*, 2014). The crystal structure of $\beta$-1,3-glucanosyltransferase from GH family 72 has been reported, along with detailed structure–activity information (Hurtado-Guerrero *et al.*, 2009).

To date, GH family 17 contains 1300 members, which are widely distributed in fungi, higher plants and bacteria (http://www.cazy.org/GH17.html). These mainly include enzymes that hydrolyze $\beta$-1,3 linkages in glucans, as found in laminarin (endo-$\beta$-1,3-glucanase; EC 3.2.1.39) and lichenan (endo-$\beta$-1,3–1,4-glucanase; EC 3.2.1.73). $\beta$-1,3-Glucanosyltransferase activity has also been reported for some GH family 17 enzymes from fungi (*A. fumigatus*; Mouyna *et al.*, 1998; Gastebois *et al.*, 2010) and yeasts (*Candida albicans* and *Saccharomyces cerevisiae*; Klebl & Tanner, 1989; Hartland *et al.*, 1991; Goldman *et al.*, 1995; Sarthy *et al.*, 1997; Sestak *et al.*, 2004). The catalytic mechanism of these enzymes can be described as a 'two-step' retaining mechanism: the first step is the cleavage of $\beta$-1,3-glucan or related oligosaccharides at a $\beta$-1,3 linkage, releasing laminaribiose from the reducing end of the linear substrates; the second step is to transfer the remaining glucan (or a related oligosaccharide) to another $\beta$-1,3-glucan (or a related oligosaccharide) acceptor with a $\beta$-1,6 linkage (Goldman *et al.*, 1995; Mouyna *et al.*, 1998; Gastebois *et al.*, 2010). Because of their action on $\beta$-1,3-glucans, these enzymes may play a role in structural modification of the cell wall and favour the emergence of a germ tube or an accessory hypha in yeast and fungi (Mouyna *et al.*, 2013). The role of $\beta$-1,3-glucanosyltransferase in cell-wall biosynthesis has made it a target for research into new antifungal drugs (Mouyna *et al.*, 2000; Douglas, 2001). Furthermore, owing to its transglycosylation activity, $\beta$-1,3-glucanosyltransferase also shows potential for application in the synthesis of oligosaccharides for medical and other purposes.

GH family 17 belongs to GH clan A, in which the basic structural fold is the $(\beta/\alpha)_8$ TIM-barrel with two conserved glutamate residues at the C-terminal end of $\beta$-strands 4 and 7, which serve as a proton donor and a nucleophile, respectively (Varghese *et al.*, 1994). To date, coordinates for the structures of only five GH family 17 proteins have been deposited in the Protein Data Bank. All of the reported structures of GH family 17 proteins are from plants, including endo-$\beta$-1,3-glucanases from *Hevea brasiliensis* (PDB entries 4hpg and 4iis; Rodríguez-Romero *et al.*, 2014), *Hordeum vulgare* (PDB entry 1ghs; Varghese *et al.*, 1994), *Musa acuminata* (PDB entry 2cyg; Receveur-Bréchot *et al.*, 2006) and *Solanum tuberosum* (PDB entries 3ur7, 3ur8, 4gzi and 4gzj; Wojtkowiak *et al.*, 2012, 2013) and an endo-$\beta$-1,3–1,4-glucanase from *H. vulgare* (PDB entries 1ghr and 1aq0; Varghese *et al.*, 1994; Müller *et al.*, 1998). However, there is no available structural information for $\beta$-1,3-glucanosyltransferases of GH family 17. Although the GH family 17 members share a similar overall fold and active-site topology, $\beta$-1,3-glucanosyltransferases have a significantly different catalytic function and very low sequence similarity. Thus, these novel members of GH family 17 are still under investigation and will hopefully yield new insights into substrate binding and the catalytic mechanism.

*Rhizomucor miehei* CAU432 is a thermophilic fungus that thrives at an optimum temperature of 323 K (Tang *et al.*, 2012). To elucidate the catalytic mechanism of the GH family 17 $\beta$-1,3-glucanosyltransferase from *R. miehei* CAU432 (*Rm*Bgt17A), this enzyme was subjected to crystallization and diffraction. In the present study, we report the crystal structures of *Rm*Bgt17A and of two complexes with laminaribiose and laminaripentaose. We also tested the specific activities of this enzyme and its mutants. Our results provide new information towards elucidating the exact mode of action of this enzyme.

## 2. Materials and methods

### 2.1. Cloning, expression and purification

We have reported the genome of *R. miehei* CAU432 in order to explore the thermostable enzymatic repertoire of this fungus (Zhou *et al.*, 2014). In this study, we identified a novel GH family 17 $\beta$-1,3-glucanosyltransferase (*Rm*Bgt17A) gene from *R. miehei* CAU432. The *Rm*Bgt17A cDNA sequence was deposited in the GenBank nucleotide-sequence database with accession No. KP121406. To express the gene in *Escherichia coli*, the open reading frame (ORF) was amplified by PCR with primers *Rm*Bgt17A-up and *Rm*Bgt17A-down (Supplementary Table S1) from the genomic DNA of *R. miehei* CAU432. BamHI and XhoI sites were added to the forward and reverse primers, respectively. The purified PCR products were digested with BamHI and XhoI, and subcloned into the pET-28a(+) vector (Novagen). The identity of the recombinant plasmid was confirmed by DNA sequencing. E189A, E158A, Y102A, W157A and W157F mutants were generated using a Fast Mutagenesis System site-directed mutagenesis kit (TransGen Biotech, People's Republic of China). The primers used in the site-directed mutagenesis are shown in Supplementary Table S1. All recombinant plasmids of these mutations were also sequenced and verified.

The correct recombinant plasmid was transformed into *E. coli* Rosetta (DE3) competent cells for gene expression. Seed cultures of *E. coli* Rosetta (DE3) harbouring *Rm*Bgt17A in the pET-28a(+) vector were prepared by incubating cells in LB medium containing 50 µg ml$^{-1}$ kanamycin at 37°C on a rotary shaker at 200 rev min$^{-1}$ for 4 h. When the absorbance at 600 nm of the culture broth reached 0.6–0.8, overexpression of *Rm*Bgt17A was induced by adding 1 m*M* IPTG (isopropyl $\beta$-D-1-thiogalactopyranoside). Cultures were grown at 30°C for a further 12 h and the cells were harvested by centrifugation at 10 000*g* for 10 min at 4°C. The precipitate was suspended in buffer (20 m*M* Tris–HCl pH 8.0, 500 m*M* NaCl)

**Table 1**
X-ray data-collection and refinement statistics.

| | SeMet *Rm*Bgt17A | *Rm*Bgt17A–L2 | *Rm*Bgt17A–L5 |
|---|---|---|---|
| Data-collection statistics | | | |
| Radiation source | BL17U, SSRF | 3W1A, BSRF | 3W1A, BSRF |
| Wavelength (Å) | 0.9792 | 0.9791 | 0.9791 |
| Temperature of measurements (K) | 100 | 100 | 100 |
| Resolution (Å) | 27.49–1.30 (1.35–1.30) | 49.92–2.27 (2.35–2.27) | 50.20–2.30 (2.39–2.30) |
| Space group | $P2_12_12_1$ | $P2_12_12_1$ | $P2_12_12_1$ |
| Unit-cell parameters (Å) | $a$ = 45.9, $b$ = 50.4, $c$ = 98.4 | $a$ = 46.8, $b$ = 52.8, $c$ = 99.8 | $a$ = 46.8, $b$ = 52.4, $c$ = 100.4 |
| Protein molecules in asymmetric unit | 1 | 1 | 1 |
| Unique reflections | 52655 (3766) | 11391 (993) | 11212 (930) |
| Completeness (%) | 92.39 (67.05) | 94.89 (84.01) | 98.11 (83.11) |
| $R_{merge}$† (%) | 8.5 (32.8) | 8.6 (18.4) | 7.8 (21.7) |
| Mean $I/\sigma(I)$ | 71.50 (8.78) | 15.62 (6.17) | 15.02 (4.19) |
| Wilson $B$ factor (Å$^2$) | 13.87 | 24.36 | 24.90 |
| Refinement statistics | | | |
| Resolution (Å) | 1.30 | 2.27 | 2.30 |
| $R_{work}$‡ (%) | 15.78 (22.37) | 19.90 (22.05) | 19.62 (24.11) |
| $R_{free}$‡ (%) | 17.82 (22.39) | 23.72 (22.08) | 21.86 (28.00) |
| No. of residues | 266 | 266 | 266 |
| No. of water molecules | 227 | 124 | 142 |
| No. of atoms | 2383 | 2249 | 2241 |
| R.m.s.d. | | | |
| Bond lengths (Å) | 0.010 | 0.017 | 0.018 |
| Bond angles (°) | 1.37 | 1.70 | 1.67 |
| Average $B$ factors (Å$^2$) | | | |
| Overall | 17.50 | 22.40 | 21.30 |
| Macromolecules | 16.50 | 21.60 | 20.60 |
| Ligands | 22.30 | 39.30 | 35.20 |
| Solvent | 26.30 | 29.30 | 28.70 |
| Ramachandran plot | | | |
| Most favoured regions (%) | 96.94 | 96.51 | 96.51 |
| Additional allowed regions (%) | 2.62 | 3.10 | 3.10 |
| Disallowed regions (%) | 0.44 | 0.39 | 0.39 |
| Clashscore§ | 5.17 | 1.20 | 3.40 |
| PDB code | 4wtp | 4wtr | 4wts |

† $R_{merge} = \sum_{hkl}\sum_i |I_i(hkl) - \langle I(hkl)\rangle| / \sum_{hkl}\sum_i I_i(hkl)$, where $I_i(hkl)$ is the $i$th observation of reflection $hkl$ and $\langle I(hkl)\rangle$ is the weighted average intensity for all observations $i$ of reflection $hkl$. ‡ $R_{work}/R_{free} = \sum_{hkl} ||F_{obs}| - |F_{calc}|| / \sum_{hkl} |F_{obs}|$; around 1000–1200 reflections were used for the calculation of $R_{free}$. § Clashscore was obtained using the validation tools in *MolProbity* (Chen *et al.*, 2010).

and disrupted by sonication. The debris was removed by centrifugation at 10 000*g* for 5 min and the clear supernatant was applied onto an Ni–IDA column (1 × 5 cm; GE Life Sciences, USA) pre-equilibrated with buffer *A* (50 m*M* Tris–HCl pH 8.0, 500 m*M* NaCl, 20 m*M* imidazole). The column was washed with 15 column volumes (CV) of buffer *A* followed by 5 CV of buffer *B* (50 m*M* Tris–HCl pH 8.0, 500 m*M* NaCl, 50 m*M* imidazole) and 5 CV of buffer *C* (50 m*M* Tris–HCl pH 8.0, 500 m*M* NaCl, 200 m*M* imidazole) at a flow rate of 1.0 ml min$^{-1}$. The eluted proteins were fractionally collected and checked by SDS–PAGE. To remove the His tag, *Rm*Bgt17A (1 mg ml$^{-1}$) was incubated with trypsin (0.01 mg ml$^{-1}$; Amresco, USA) in 100 m*M* Tris–HCl pH 8.0 at 293 K overnight. The protein was further purified by gel filtration on a Sephacryl S-100 HR column in buffer *D* (20 m*M* Tris–HCl pH 8.0, 100 m*M* NaCl). The purified protein fractions were combined and concentrated for subsequent experiments. All mutant genes were expressed and the corresponding recombinant proteins were purified following the same method. Selenomethionine-derivatized *Rm*Bgt17A (SeMet *Rm*Bgt17A) was produced using a metabolic inhibition protocol with M9 medium supplemented with 50 mg l$^{-1}$ L-selenomethionine and was purified using the same protocol.

### 2.2. Crystallization and data collection

*Rm*Bgt17A was concentrated to 15 mg ml$^{-1}$ in buffer *D*. Crystallization experiments were performed in 48-well plates by the sitting-drop vapour-diffusion method at 293 K, and each sitting drop was prepared by mixing 1 µl each of protein solution and reservoir solution. Crystals of *Rm*Bgt17A were obtained with a reservoir solution consisting of 25%(*w*/*v*) polyethylene glycol (PEG) 8000, 0.2 *M* ammonium sulfate. The crystals were observed after 3 d. As no homologous structure of a member of the GH family 17 $\beta$-1,3-glucanosyltransferases has been determined, experimental phasing was necessary. Thus, SeMet *Rm*Bgt17A was prepared and concentrated to 15 mg ml$^{-1}$ in buffer *D*, and crystals of SeMet-derivatized protein were obtained with the reservoir solution used for the uncomplexed native protein. To obtain complex crystals, we first attempted to co-crystallize the E189A mutant with oligosaccharides, but this was not successful. Complex crystals were ultimately obtained by oligosaccharide-soaking experiments. A laminaribiose complex crystal (*Rm*Bgt17A–L2) was obtained by adding 20%(*w*/*v*) laminaribiose to the reservoir solution and soaking the E189A mutant crystals in it for 48 h. Similarly, a laminaripentaose complex crystal (*Rm*Bgt17A–L5) was obtained by soaking the E189A mutant crystals in reservoir solution containing 12%(*w*/*v*) laminaripentaose for 48 h.

For X-ray diffraction experiments, each crystal was fished out from the crystallization drop using a nylon loop (Hampton Research), soaked briefly in a cryoprotectant solution [the crystallization solution supplemented with 20%(*v*/*v*) glycerol] and flash-cooled in liquid nitrogen at 70 K. Single-wavelength anomalous dispersion (SAD) data were collected to 1.3 Å resolution for the SeMet *Rm*Bgt17A crystal at a wavelength of 0.9792 Å, the absorption edge of selenium, on beamline BL17U at the Shanghai Synchrotron Research Facility (SSRF). X-ray diffraction data sets for the *Rm*Bgt17A–L2 and *Rm*Bgt17A–L5 complex crystals were collected to 2.30 and 2.27 Å resolution, respectively, on beamline 3W1A at the Beijing Synchrotron Radiation Facility (BSRF). All diffraction data were indexed, integrated and scaled using *HKL*-2000 (Otwinowski & Minor, 1997).

The SeMet *Rm*Bgt17A crystal system was orthorhombic (space group $P2_12_12_1$), with unit-cell parameters $a$ = 45.9, $b$ = 50.4, $c$ = 98.4 Å. The *Rm*Bgt17A–L2 and *Rm*Bgt17A–L5 crystals were nearly isomorphous to the SeMet *Rm*Bgt17A crystal, with the same space group $P2_12_12_1$ and similar unit-cell parameters.

### 2.3. Phase determination, model building and refinement

The structure of uncomplexed *Rm*Bgt17A was determined at 1.30 Å resolution by anomalous signal (Se-SAD) phasing techniques using the SeMet *Rm*Bgt17A crystal. For phasing experiments, *phenix.hyss* (Adams *et al.*, 2010) was used to determine the selenium substructure, *phenix.phaser* (McCoy *et al.*, 2007) was used for phasing, *phenix.resolve* (Terwilliger & Berendzen, 1999) was used for density modification and *phenix.autobuild* was used for automatic model building (Adams *et al.*, 2010). The structure was completed with alternating rounds of manual model building with *Coot* (Emsley *et al.*, 2010) and refinement with *phenix.refine* (Afonine *et al.*, 2012). The uncomplexed crystal structure was further refined with anisotropic ADPs by *REFMAC*5 (Murshudov *et al.*, 2011). Structural homologues of *Rm*Bgt17A were identified by the *DALI* server (Holm & Rosenström, 2010). Structural superposition and r.m.s.d. calculations were performed in *LSQMAN* (Kleywegt, 1999). Secondary-structure elements were identified by *DSSP* (Kabsch & Sander, 1983). The figures were prepared in *PyMOL* (v.1.3; Schrödinger). The sequence alignments were created with *MUSCLE* (McWilliam *et al.*, 2013) and *ESPript* (Robert & Gouet, 2014). Data-collection and refinement statistics are given in Table 1. To provide a structural explanation for the formation of a $\beta$-1,6 linkage, the transglycosylation product octasaccharide was docked using *GOLD* v.2.1 (CCDC Software Ltd, Cambridge, England; Verdonk *et al.*, 2003). The crystal structure of the uncomplexed *Rm*Bgt17A was chosen as the template for the docking study.

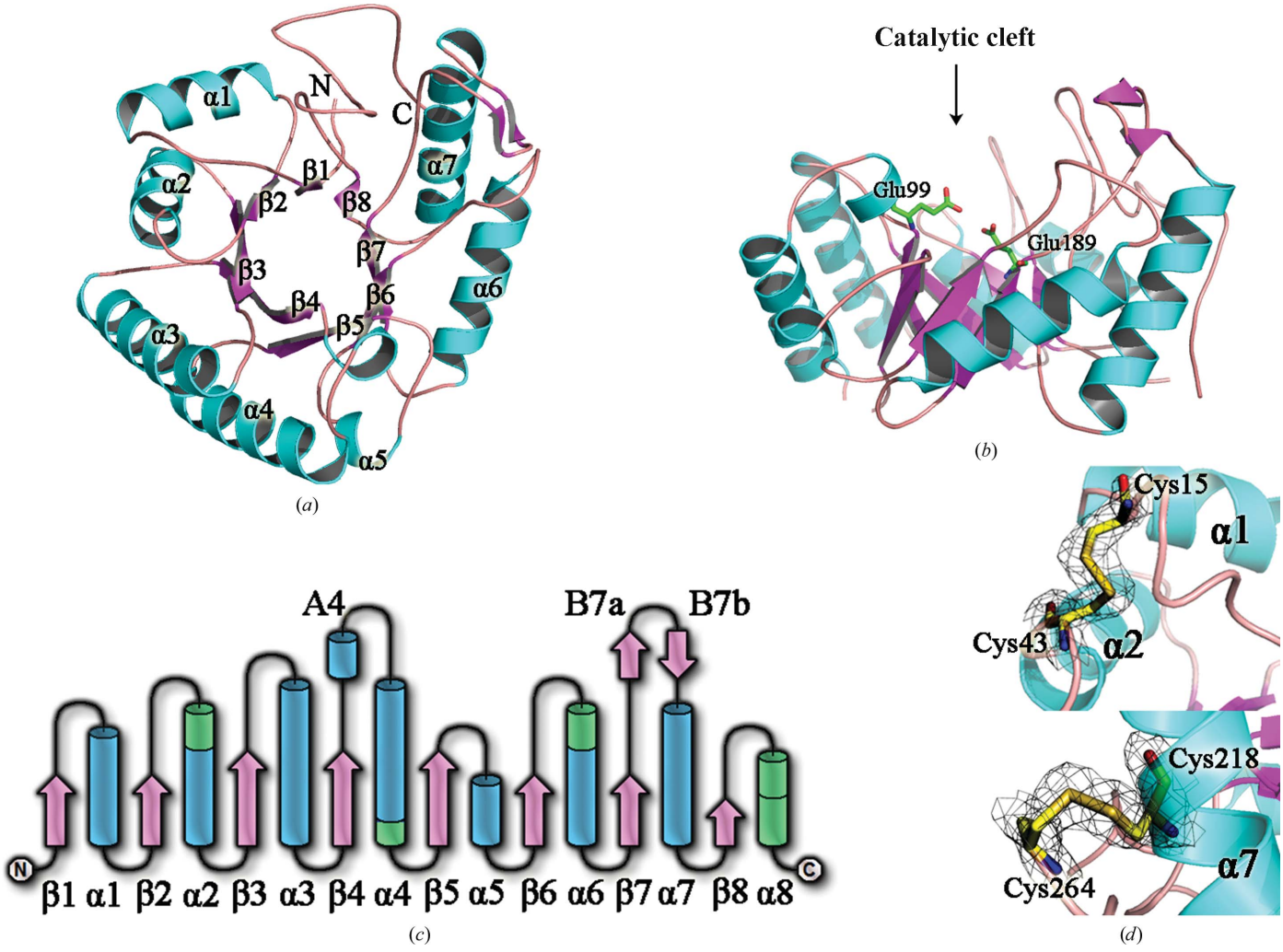


**Figure 1**
The overall structure of *Rm*Bgt17A is shown as a ribbon diagram, illustrating the classical $(\beta/\alpha)_8$ TIM-barrel. The $\beta$-strands (purple) of the inner $\beta$-barrel are surrounded by $\alpha$-helices (cyan) linked by a loop region (pink). (*a*) Top view down the TIM-barrel axis. (*b*) Side view of the molecule, with the catalytic cleft facing the viewer. (*c*) Topology diagram of *Rm*Bgt17A. Colour code: purple, $\beta$-strand; cyan, $\alpha$-helix; green, $3_{10}$-helix. (*d*) The electron densities of two intramolecular disulfide bonds are shown as the $\sigma_A$-weighted $mF_o - DF_c$ OMIT map contoured at the 3.0$\sigma$ level.

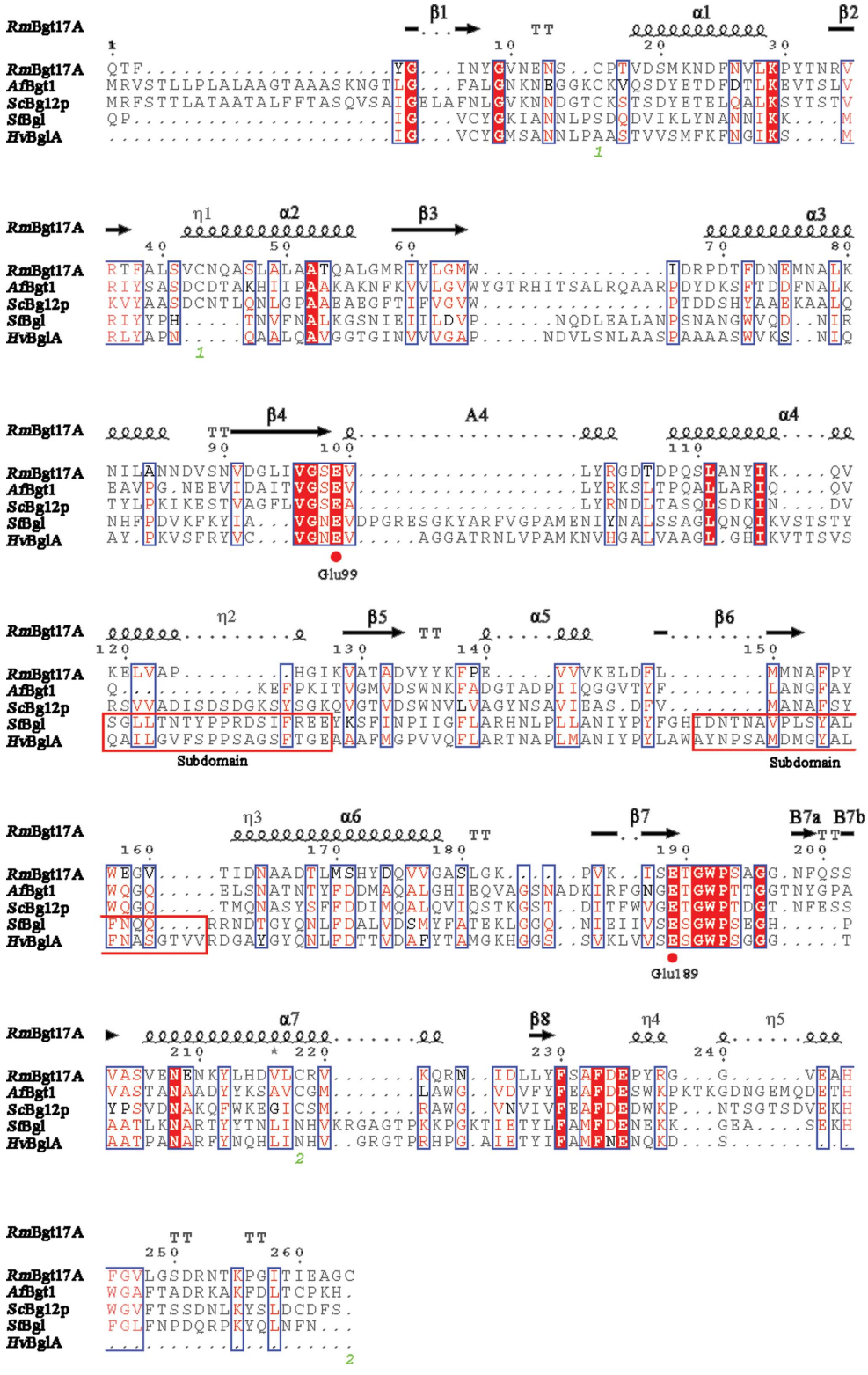


Figure 2
Structural sequence alignment of some GH family 17 members. Identical residues are shown in white on a red background and conservative residues are shown in red on a white background. Two catalytic glutamic acid residues, Glu99 and Glu189, are marked by red dots. The sequences of *Rm*Bgt17A, *A. fumigatus* β-1,3-glucanosyltransferase (*Af*Bgt1), *S. cerevisiae* β-1,3-glucanosyltransferase (*Sc*Bgl12p), *S. tuberosum* endo-1,3-β-glucanase (*St*Bgl; PDB entry 3ur8) and *H. vulgare* endo-1,3–1,4-β-glucanase (*Hv*BglA; PDB entry 1aq0) were aligned by *MUSCLE* and the figure was produced in *ESPript*. The subdomain regions of *St*Bgl and *Hv*BglA are indicated by red boxes.

### 2.4. Enzyme assay and transglycosylation properties

Transglycosylation activity was quantitated by high-performance anion-exchange chromatography (HPAEC) using laminaripentaose as the substrate and an octasaccharide as the product. One unit of enzyme activity was defined as the amount of enzyme required to produce 1 µmol octasaccharide per minute under the following conditions: 4 µl of suitably diluted enzyme was mixed with 36 µl of 2%(*w*/*v*) laminaripentaose in 50 m*M* sodium acetate buffer pH 4.5. The reaction mixture was incubated at 50°C for 15 min and the reaction was then terminated by boiling for 10 min. The mixture was diluted 50-fold with 100 m*M* NaOH and analyzed by HPAEC (ICS-5000$^+$, Dionex, USA) with amperometric detection (PAD) on a CarboPac PA10 (4 × 250 mm) preparative column (Dionex) with a 0–350 m*M* sodium acetate gradient in 100 m*M* NaOH (20 min) at a flow rate of 1 ml min$^{-1}$.

The transglycosylation products derived from laminaripentaose and laminarihexaose were analyzed by matrix-assisted laser desorption ionization/time-of-flight mass spectrometry (MALDI-TOF MS). The enzyme (10 µg) was incubated with 0.5%(*w*/*v*) laminaripentaose or laminarihexaose in 50 m*M* sodium acetate buffer pH 4.5 at 50°C for 2 h (20 µl assay volume). For analysis, the sample was diluted 100-fold prior to mixing with an equal volume of matrix (2,5-dihydroxybenzoic acid, 10 mg ml$^{-1}$ in water). The sample (1 µl) was then spotted onto the MALDI plate and analyzed using an AB SCIEX TOF/TOF 5800 System operated in positive-ion mode.

For structural analysis of the octasaccharide, a transglycosylation reaction (20 ml) was

performed with 10 mg *Rm*Bgt17A, 1%(*w*/*v*) laminaripentaose at 50°C for 2 h. The transglycosylation product was purified by silica-gel column chromatography (16 × 800 mm) and eluted with 4:2:1 ethyl acetate:methanol:water at a flow rate of 1 ml min$^{-1}$. The purified octasaccharide (~10 mg) was freeze-dried and dissolved in deuterium oxide (500 µl) prior to recording spectra on a Bruker Avance 500 NMR spectrometer. One-dimensional $^{1}$H and $^{13}$C spectra were acquired using standard pulse sequences.

### 2.5. PDB accession codes

The atomic coordinates and structure factors for the crystal structures of *Rm*Bgt17A and its oligosaccharide complexes have been deposited in the PDB (Research Collaboratory for Structural Bioinformatics, Rutgers University, New Brunswick, New Jersey, USA; http://www.pdb.org) with accession codes 4wtp, 4wtr and 4wts.

## 3. Results and discussion

### 3.1. Overall structure

The overall structure of uncomplexed *Rm*Bgt17A is presented in Fig. 1. The crystal structure of *Rm*Bgt17A was determined at 1.30 Å resolution in space group $P2_12_12_1$. $R_{work}$ and $R_{free}$ were 15.78 and 17.82%, respectively. The protein molecule, with approximate dimensions of 50 × 44 × 30 Å, exhibited a single-domain architecture consisting of residues −1 to 264. The His tag was removed by trypsin. Gly−1 and Ser0 were two extra residues translated from the pET-28a(+) plasmid which are also visible in the electron-density map. The overall structure of *Rm*Bgt17A exhibited the $(\beta/\alpha)_8$ TIM-barrel fold characteristic of all GH family 17 members (Figs. 1*a* and 1*b*), consisting of an internal core of eight $\beta$-strands connected by more or less extended loops to an external layer of eight $\alpha$-helices. However, in contrast to the classical $(\beta/\alpha)_8$ TIM-barrel, two short antiparallel $\beta$-strands (B7a and B7b) were located in the loop between $\beta$7 and $\alpha$7, and a short $\alpha$-helix (A4) was located in the loop between $\beta$4 and $\alpha$4 (Fig. 1*c*). The protein featured a roughly V-shaped groove which, by structural homology to other GH family 17 members, corresponded to the catalytic cleft containing the catalytic proton donor and nucleophile (Glu99 and Glu189, respectively). This central groove, of approximately 33 Å in length, lay between $\alpha$2 and $\alpha$3 at the N-terminus of the protein and between $\alpha$5 and $\alpha$6 at its C-terminus. *Rm*Bgt17A contained two disulfide bonds: Cys15–Cys43 (Cys15 is in the loop near the N-terminus of $\alpha$1 and Cys43 is in the short $3_{10}$-helix near the N-terminus of $\alpha$2) and Cys218–Cys264 (Cys218 is in the middle of $\alpha$7 and Cys264 is at its C-terminus) (Fig. 1*d*). Cys15 and Cys43 are strictly conserved in $\beta$-1,3-glucanosyltransferases, but are not found in other members of GH family 17 (Fig. 2). Interestingly, Cys264 is located at the C-terminus of the protein, potentially reducing the flexibility of the C-terminal loop.

### 3.2. Structural comparisons

*Rm*Bgt17A shares very low amino-acid sequence identity with other structurally characterized proteins in the PDB. A *DALI* search of *Rm*Bgt17A against the PDB showed four similar structures: *H. vulgare* endo-$\beta$-1,3–1,4-glucanase (PDB

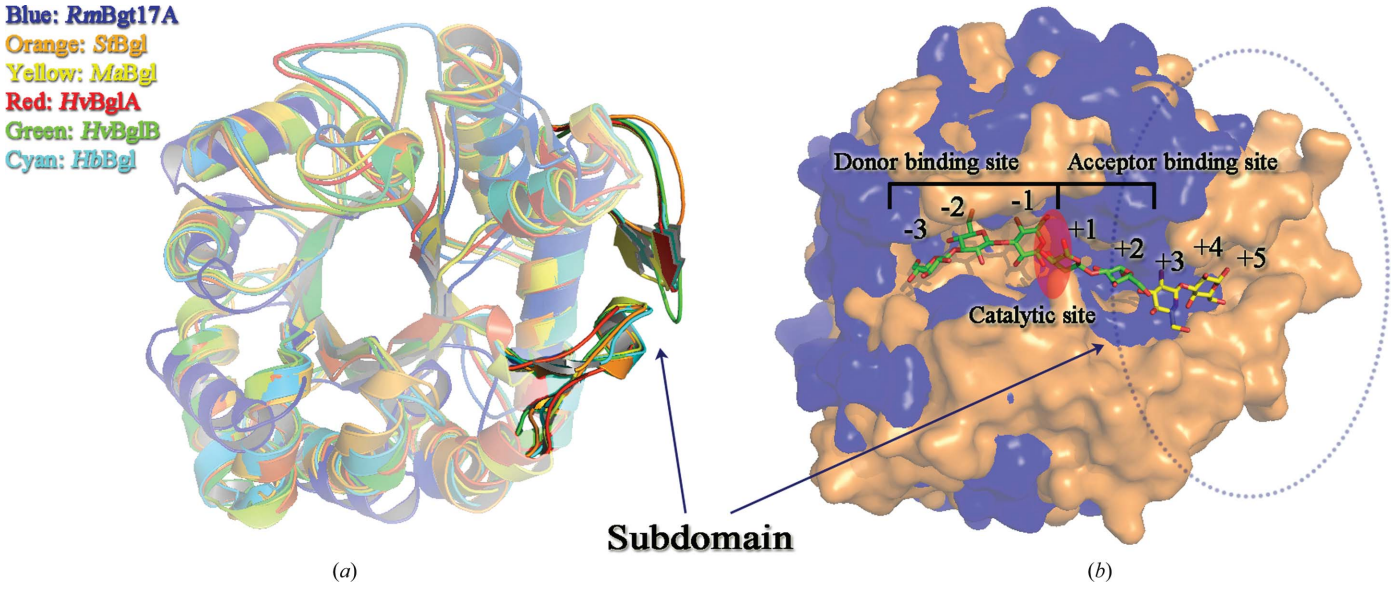


**Figure 3**
Comparison of *Rm*Bgt17A with other GH family 17 enzymes. (*a*) The superposition of *Rm*Bgt17A on other GH family 17 enzymes is shown as a ribbon diagram, with ribbons coloured according to enzyme: *Rm*Bgt17A in blue, *St*Bgl in orange, *M. acuminata* endo-1,3-$\beta$-glucanase (*Ma*Bgl; PDB entry 2cyg) in yellow, *Hv*BglA in red, *H. vulgare* endo-1,3-$\beta$-glucanase (*Hv*BglB; PDB entry 1ghs) in green and *H. brasiliensis* endo-1,3-$\beta$-glucanase (*Hb*Bgl; PDB entry 4hpg) in cyan. The conserved subdomains in GH family 17 enzymes are shown in enhanced colours. (*b*) Superposition of *Rm*Bgt17A (blue) on *St*Bgl shown as a surface diagram. The glucose residues occupying the catalytic cleft are shown as sticks. Glucose residues (subsites −3 to +2) from *Rm*Bgt17A–L2 and *Rm*Bgt17A–L5 are coloured green. Glucose residues (subsites +3 and +4) from the *St*Bgl–7G complex (PDB entry 4gzj) are coloured yellow. The catalytic site and the donor and acceptor binding site regions are labelled.

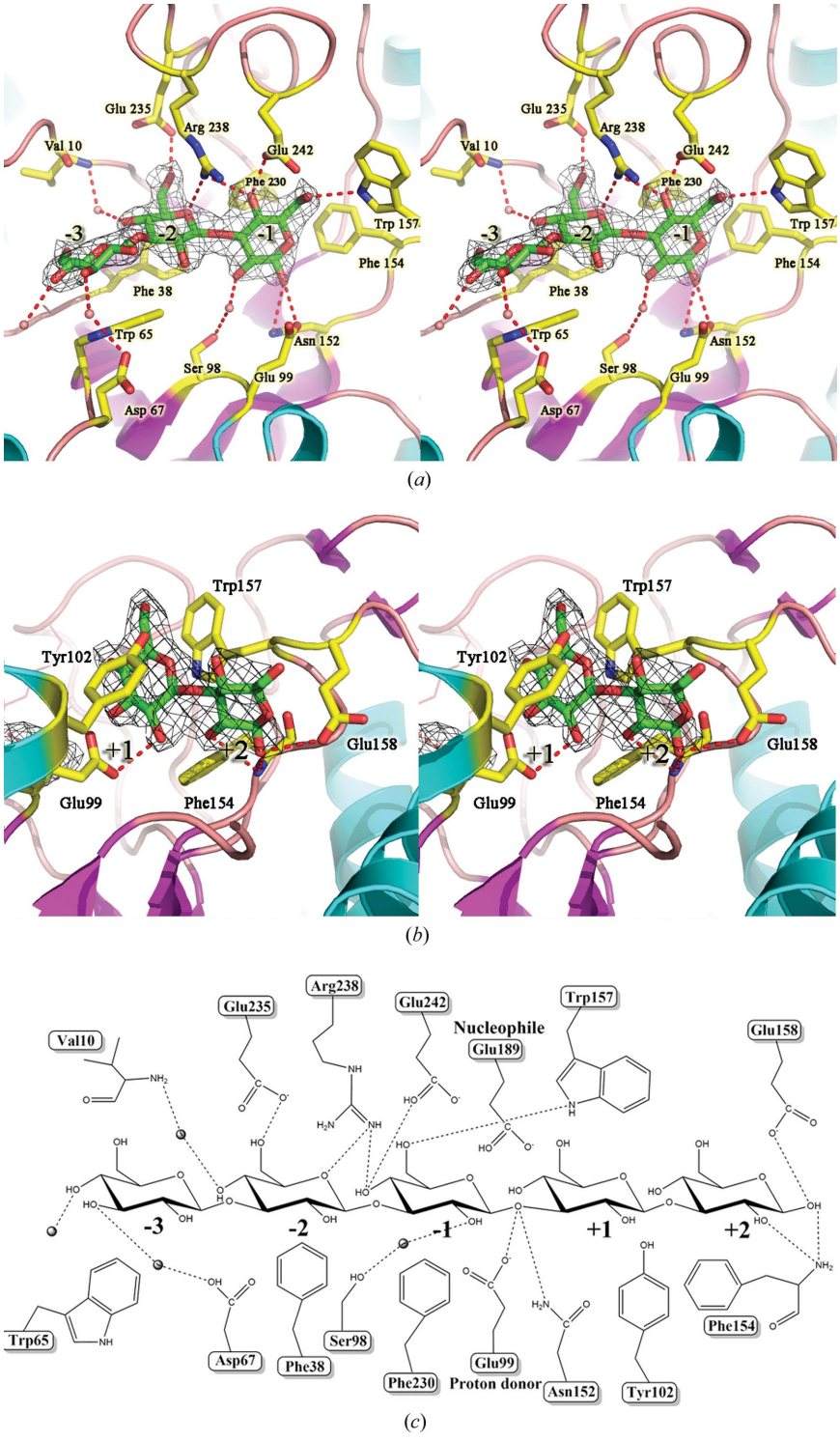


**Figure 4**
Substrate interactions of *Rm*Bgt17A. (*a*) Stereoview of the substrate interactions in subsites −3, −2 and −1 of *Rm*Bgt17A–L5. The trisaccharide ligand bound at subsites −1, −2 and −3 of the protein is shown as green/red sticks. (*b*) Stereoview of the substrate interactions in subsites +1 and +2 of *Rm*Bgt17A–L2. The disaccharide ligand bound at subsites +1 and +2 of the protein is shown as green/red sticks. The key protein residues are shown in yellow and hydrogen bonds are indicated by red dotted lines. Water molecules are shown as red spheres. The electron density of the trisaccharide ligand is shown as a $\sigma_A$-weighted $mF_o - DF_c$ OMIT map contoured at the 3.0$\sigma$ level. The occupancy of the oligosaccharide ligands in the complex structures is 100%. (*c*) Schematic representation of substrate interactions of *Rm*Bgt17A. The oligosaccharide is shown as sticks. The hydrogen-bonding interactions are shown as dotted lines.

entry 1aq0), *H. vulgare* endo-$\beta$-1,3-glucanase (PDB entry 1ghs), *S. tuberosum* endo-$\beta$-1,3-glucanase (PDB entry 3ur8) and *M. acuminata* endo-$\beta$-1,3-glucanase (PDB entry 2cyg), with *Z*-scores of 24.2, 24.0, 23.6 and 23.6 and r.m.s.d. values of 2.2, 2.3, 2.5 and 2.4 Å, respectively. Superposition of *Rm*Bgt17A on the reported GH family 17 enzyme structures (Fig. 3*a*) showed several differences in the overall folding of the former. These structural differences were mainly located in the loop regions and in the substructure alongside the classical $(\beta/\alpha)_8$ TIM-barrel. An additional helix between $\beta$3 and $\alpha$3, which is conserved in GH family 17 (Müller *et al.*, 1998), was absent in *Rm*Bgt17A. Instead, a single additional small helix between $\beta$4 and $\alpha$4 was present in *Rm*Bgt17A but did not exist in other GH family 17 members. The most important structural difference between *Rm*Bgt17A and other GH family 17 members was the absence in the former of a strictly conserved subdomain found in classical GH family 17 members (Figs. 3*a* and 3*b*). In the endo-$\beta$-1,3–1,4-glucanase (PDB entry 1aq0), this subdomain is built around helix $\alpha$6 at the end of the catalytic cleft, which is supported by two short antiparallel $\beta$-strands between $\beta$6 and $\alpha$6, two short $\alpha$-helices between $\beta$5 and $\alpha$5, and the neighbouring loops. This conserved subdomain plays a key role in binding long-chain substrate in the catalytic cleft (Fig. 3*b*) and could provide subsites +3, +4 and +5 in the plant $\beta$-1,3-glucanase (Wojtkowiak *et al.*, 2013). The lack of this subdomain implies that *Rm*Bgt17A has a unique substrate-binding mode.

### 3.3. Crystal structures of *Rm*Bgt17A complexes

The structure of *Rm*Bgt17A/E189A in complex with laminaripentaose (*Rm*Bgt17A–L5) was determined at 2.30 Å resolution (Fig. 4*a*). Only three glucose units (laminaritriose) linked by $\beta$-1,3 glycosidic bonds could be built into electron density (at subsites −3 to −1), with the nonreducing terminus at the end of the catalytic cleft (subsite −3) surrounded by the loop between $\beta$2 and $\alpha$2. The lack of electron density for glucose moieties at subsites +1 and +2 in the laminaripentaose might be owing to the following: (i) the glucoses in subsites +1 and +2 are very flexible and (ii) the enzyme assay showed that the E189A

Table 2
Transglycosylation activity of wild-type and mutants of *Rm*Bgt17A.

| *Rm*Bgt17A | Specific activity (U mg$^{-1}$) | Relative activity (%) |
|---|---|---|
| Wild type | 2.45 ± 0.04 | 100 |
| Glu189Ala | 0.03 ± 0.002 | 1.22 |
| Tyr102Ala | None† | 0 |
| Glu158Ala | None | 0 |
| Trp157Phe | 0.35 ± 0.01 | 14.29 |
| Trp157Ala | None | 0 |

† No activity was detected.

mutant still has some residual transglycosylation activity (Table 2) and these +1 and +2 glucose residues might have been slowly cleaved by *Rm*Bgt17A/E189A during the soaking process.

In addition, a crystal structure of *Rm*Bgt17A/E189A in complex with laminaribiose (*Rm*Bgt17A–L2) was solved at 2.27 Å resolution. The laminaribiose was found to occupy the catalytic cleft of *Rm*Bgt17A. Remarkably, two laminaribioses (at subsites −3/−2 and +1/+2) were well defined in the electron-density maps, except for C6 and the corresponding hydroxyl group of the +2 glucose (Fig. 4*b*). All four glucose residues adopted the relaxed chair conformation $^4C_1$. The −3, −2 glucose residues of *Rm*Bgt17A–L2 and the −3, −2 glucose residues of *Rm*Bgt17A–L5 were in almost the same position. Superposition of *Rm*Bgt17A–L5 or *Rm*Bgt17A–L2 on the uncomplexed structure of *Rm*Bgt17A showed that most of the residues in the catalytic cleft are in the same positions. However, the side chains of residues in the $\beta$8–$\alpha$8 loop and the neighbouring $3_{10}$-helix (Tyr237, Arg238 and Glu242) displayed significant variation. This loop region showed high *B* factors in its overall structure, indicating that it was flexible during the process of substrate recognition and binding.

### 3.4. The catalytic cleft and the active site

An approximately 33 Å long and 8–9 Å deep catalytic cleft was located on the upper surface of the *Rm*Bgt17A molecule, allowing the binding of carbohydrates. The centre of this cleft exhibited a pronounced electronegative character owing to the presence of Glu99, Glu189 and Glu242. Two strictly conserved catalytic glutamate residues, Glu99 and Glu189, lie one-third of the way down the cleft, acting as a proton donor and a nucleophile, respectively. Based on the complex structures, oligosaccharides were located in the catalytic cleft occupying subsites −3 to +2 (Fig. 4). In both the *Rm*Bgt17A–L5 and *Rm*Bgt17A–L2 structures, subsites −3 and −2 were occupied by glucose residues, all of which adopted the relaxed chair conformation $^4C_1$. This arrangement may represent the conformation of transglycosylation reactants, with the −3 to −1 sugars representing the donor sites and the +1 and +2 sugars representing the acceptor sites.

The −3 to −1 glucose residues formed direct hydrogen bonds to Glu99, Asn152, Glu235, Arg238, Glu242 and Trp157. Water-mediated hydrogen bonds were formed to Val10, Asp67 and Ser98 (Fig. 4*c*). The O6 hydroxyl of the −2 glucose residue was directly hydrogen-bonded to the $O^{\varepsilon2}$ atom of Glu235, which is part of the $\beta$8–$\alpha$8 loop and is strictly conserved in the GH family 17 enzymes. The O5 hydroxyls of the −2 glucose residue were directly hydrogen-bonded to the $N^{\eta1}$ atom of Arg238, which is often replaced by lysine in other GH family 17 members, playing a similar role. The −1 glucose residue was surrounded by a hydrogen-bond network with some strictly conserved residues (O1···Glu99 $O^{\varepsilon2}$, O1···Asn152 $N^{\delta2}$, O4···Arg238 $N^{\eta1}$ and O4···Glu242 $O^{\epsilon1}$). Furthermore, the O6 hydroxyl of the −1 glucose residue was directly hydrogen-bonded to the $N^{\varepsilon1}$ atom of Trp157, which is only conserved in GH family 17 $\beta$-1,3-glucanosyltransferases. The importance of the conserved residues Glu235, Arg238 and Glu242 for substrate binding was corroborated by site-directed mutagenesis of barley $\beta$-1,3-glucanase (Chen *et al.*, 1995), in which substitution of each of these residues reduced the activity of the enzyme. Several aromatic residues (Phe38, Trp65, Phe230 and Phe154) were located along the cleft. Phe38 and Trp65 stacked against the glucose units at subsites −2 and −3, forming a hydrophobic sugar-binding platform. Phe230 and Phe154 were involved in hydrophobic interactions with subsite −1. In particular, Trp65 is only conserved in GH family 17 $\beta$-1,3-glucanosyltransferases and is lacking in other enzymes of GH family 17.

The +1 and +2 glucose residues interacted with several residues (Glu99, Tyr102, Phe154, Trp157 and Glu158) of the catalytic cleft (Fig. 4*c*). There were four direct protein–ligand hydrogen bonds but no water-mediated interactions for the +1 and +2 glucose residues. The O2 hydroxyl of the +1 glucose residue and the O1 hydroxyl of the +2 glucose residue were directly hydrogen-bonded to the $O^{\varepsilon2}$ atom of Glu99 and the $O^{\varepsilon2}$ atom of Glu158, respectively. The aromatic rings of Tyr102 and Trp157, serving as the hydrophobic sugar-binding platform, made contact with the +1 glucose residue. In addition, the oligosaccharide–protein complexes showed that there is no space for a $\beta$-1,6 branch at subsites −3, −2 and −1 (Fig. 4). Therefore, a $\beta$-1,6 branch of the substrate is only possible in subsites +1 and +2.

### 3.5. The unique substrate-binding region

The topologies of the active sites in the GH superfamily can be classified into three general categories: pocket, tunnel and cleft (Davies & Henrissat, 1995). The structure of *Rm*Bgt17A shows a long cleft topology, which is an 'open' structural feature for binding polysaccharide substrates that presumably performs its catalytic function by an endo cleavage reaction. However, a distinct substrate-binding region in the +2 subsite contributes to the unique catalytic property of the GH family 17 $\beta$-1,3-glucanosyltransferases. In particular, four superficial bulky side-chain residues (Tyr135, Tyr136, Glu158 and His172) surrounded the reducing terminus of the +2 glycosyl (Fig. 5). This special pocket region creates steric hindrance near O1 of the +2 glycosyl, blocking the catalytic cleft of *Rm*Bgt17A. On the other hand, owing to the absence of a subdomain built around helix $\alpha$6 at the end of the catalytic cleft, *Rm*Bgt17A lacks the +3, +4 and +5 binding sites (Fig. 3). Therefore, the special substrate-binding region of *Rm*Bgt17A clearly explains the catalytic mode of cleaving a laminaribiose in the first

catalysis step above. Such activity has also been described in other GH family 17 $\beta$-1,3-glucanosyltransferases (Robert *et al.*, 1995; Mouyna *et al.*, 1998).

Phylogenetic analysis of the GH family 17 members generated a tree in which all 35 sequences were placed into two major clades (Supplementary Fig. S1). Clade I contains 25 sequences, including several known endo-$\beta$-1,3-glucanases and endo-$\beta$-1,3–1,4-glucanases. All clade I members are from plants. It is worth noting that all five structurally characterized enzymes of GH family 17 were placed into clade I. Clade II contains ten sequences, including all known GH family 17 $\beta$-1,3-glucanosyltransferases from fungi, yeast and bacteria (Klebl & Tanner, 1989; Mouyna *et al.*, 1998; Hreggvidsson *et al.*, 2011). Alignment of sequences from clade II indicated that all of the proteins lack the subdomain around helix $\alpha$6, which plays a key role in substrate binding at subsites +3 to +5. We therefore suggest that the clade II members of GH family 17 have $\beta$-1,3-glucanosyltransferase activity. Moreover, clade II includes four distinct $\beta$-1,3-glucanosyltransglucosidase sequences from bacteria. These members appear to code for two protein domains: a region encoding a glycoside hydrolase domain of GH family 17 and a region encoding a domain belonging to the Leloir glycosyltransferase of family GT2 (Hreggvidsson *et al.*, 2011).

### 3.6. Catalytic mechanism of *Rm*Bgt17A

The catalytic mechanism of the GH family 17 $\beta$-1,3-glucanosyltransferases can be described as a two-step retaining mechanism. The first step is to cleave a $\beta$-1,3 linkage of $\beta$-1,3-glucan or a related oligosaccharide, releasing a disaccharide unit from the reducing end of the primary substrate, and the second step is to form a $\beta$-1,6 linkage between the remaining (nonreducing end) part and another $\beta$-1,3-glucan or a related oligosaccharide (Hartland *et al.*, 1991; Mouyna *et al.*, 1998). *Rm*Bgt17A showed high transglycosylation activity towards laminaran oligosaccharides. Transglycosylation reactions on laminaripentaose and laminarihexaose were performed in acetate buffer pH 4.5 at 50°C for 2 h. The disaccharide byproduct of the enzymatic reactions was identified as laminaribiose by HPAEC (data not shown). MALDI-TOF MS analysis indicated that *Rm*Bgt17A catalyzes the transglycosylation of laminaripentaose to form octasaccharides (laminaritriose + laminaripentaose) and undecasaccharides (laminaritriose + octasaccharide) (Supplementary Fig. S2*a*). Moreover, the transglycosylation products derived from laminarihexaose were decasaccharides (laminaritetraose + laminarihexaose), tetradecasaccharides (laminaritetraose + decasaccharide) and a small quantity of octadecasaccharides (laminaritetraose + tetradecasaccharide) (Supplementary Fig. S2*b*). These results demonstrate that *Rm*Bgt17A has the catalytic activity characteristic of GH family 17 $\beta$-1,3-glucanosyltransferases, as found in previous studies (Hartland *et al.*, 1991; Mouyna *et al.*, 1998). To confirm the linkage of the transglycosylation product, the reaction product (octasaccharide) was analyzed by NMR spectroscopy (Supplementary Fig. S3). The chemical shifts in the one-dimensional $^{1}$H and $^{13}$C NMR spectra of the octasaccharide were in good agreement with the calculated data for a linear $\beta$-1,3-octasaccharide containing an intrachain $\beta$-1,6 linkage from *CASPER* (http://www.casper.organ.su.se/casper/). The $^{13}$C NMR spectrum of the octasaccharide displayed a characteristic chemical shift at 68.49 p.p.m. (Supplementary Fig. S3*c*), indicating a $\beta$-1,6 linkage in the octasaccharide.

To find a structural explanation for $\beta$-1,6 linkage formation, we performed a computer simulation to model an enzyme–octasaccharide (laminaritriose linked to laminaripentaose with a $\beta$-1,6 linkage at the reducing end) complex. The docking model placed the three glucose moieties from the nonreducing end of the octasaccharide at binding sites −3 to −1, in accordance with the sugar observed in the *Rm*Bgt17A–L5 structural model (Figs. 6*a* and 6*b*). The laminaripentaose moiety from the reducing end of the octasaccharide was partly bound to binding sites +1 and +2. This illustrates that the incoming acceptor molecule adopts a different binding mode towards the leaving group. The acceptor molecule entered the active sites and attacked the glycosyl-enzyme intermediate from the top of the catalytic cleft. It is important that the acceptor molecule bind at sites +1 and +2 in the position opposite to that of the leaving group. This architecture, leading to the reducing end of the acceptor, is not blocked by the terminus of the unique substrate-binding region (Fig. 5). The helical sugar chain (acceptor) can be above the active-site cleft. With this architecture, the C6 hydroxyl of the acceptor is close to the active site and is activated by a catalytic residue to form a $\beta$-1,6 linkage to the donor.

Although the active sites of *Rm*Bgt17A are partially similar to those of GH family 17 $\beta$-glucanases, the surprisingly high transglycosylation ability and very low hydrolysis ability of *Rm*Bgt17A might be owing to stabilizing interactions between the acceptor and the catalytic cleft subsites. The interactions

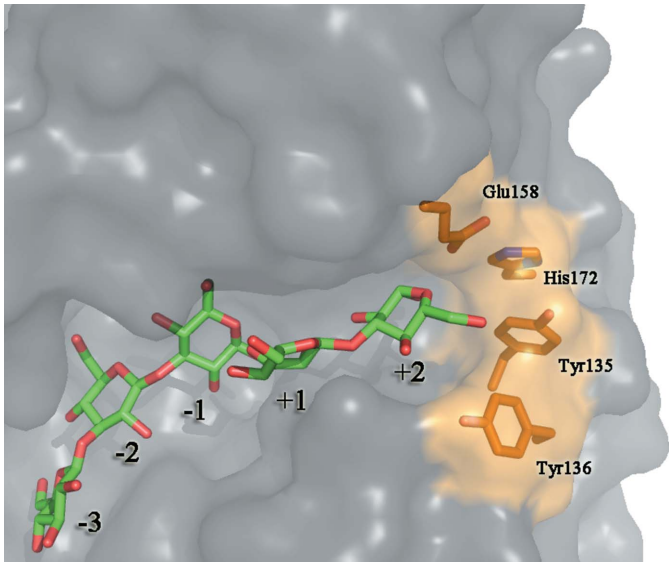


**Figure 5**
Molecular surface of the unique catalytic cleft of *Rm*Bgt17A. Amino-acid residues limiting access to the catalytic cleft are shown as sticks. The five glucose residues (grafted from the two complex structures) occupying subsites −3 to +2 are shown in green.

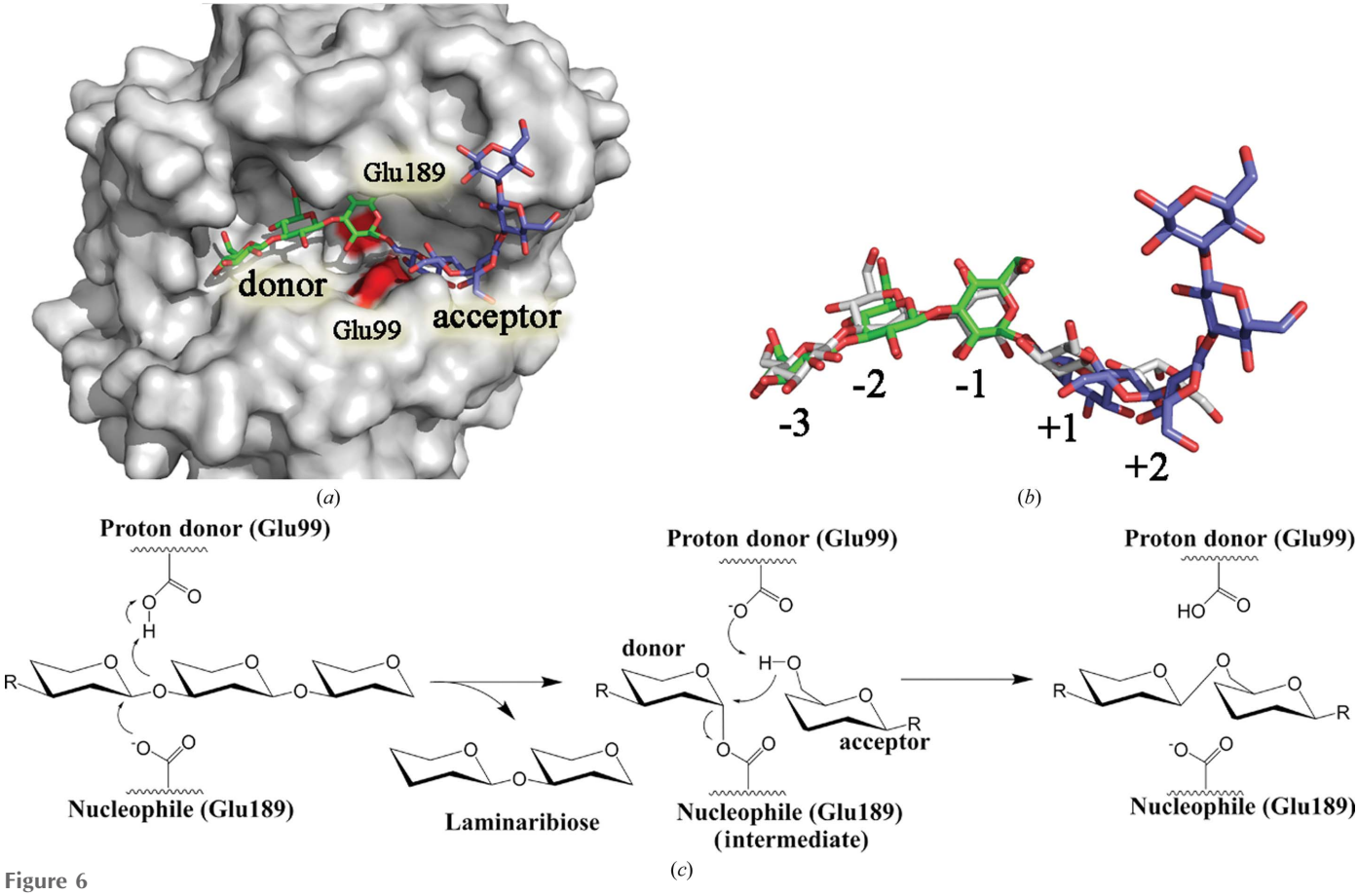


**Figure 6**
Catalytic mode of *Rm*Bgt17A transglycosylation. (*a*) The docking model of *Rm*Bgt17A bound with octasaccharide. *Rm*Bgt17A is shown as a surface view (grey). The octasaccharide is displayed as sticks. The green/red sticks indicate the donor part and the blue/red sticks indicate the acceptor part. Two catalytic residues (Glu99 and Glu189) are shown in red. (*b*) Superposition of the octasaccharide, laminaritriose and laminaribiose. The octasaccharide from the enzyme–octasaccharide docking model is shown as sticks: green/red, donor; blue/red, acceptor. The laminaritriose and laminaribiose are grafted from the two complex structures (*Rm*Bgt17A–L5 and *Rm*Bgt17A–L2, respectively) and are shown as white/red sticks. The octasaccharide and the laminaritriose/laminaribiose indicate the binding modes in the first and second steps of the catalytic reaction, respectively. (*c*) Schematic mechanism of the catalytic reaction of *Rm*Bgt17A.

that stabilize the transition state are in subsites −1, +1 and +2 for transglycosylation, but only in subsite −1 for hydrolysis (Street *et al.*, 1992; Teze *et al.*, 2014). Trp157 was directly hydrogen-bonded to the O6 hydroxyl of the −1 glucose residue and could stabilize the transition state for both transglycosylation and hydrolysis. Moreover, Trp157 and Tyr102 provide hydrophobic sugar-binding platforms in subsite +1. The conserved residue Glu158 could form direct hydrogen bonds to the transglycosylation receptor. Site-directed mutagenesis results showed that the Y102A, E158A and W157A mutants lost all of their transglycosylation ability, while the W157F mutant retained only 14.29% of the wild-type transglycosylation activity (Table 2). These special structural features stabilize the transglycosylation transition state and endow *Rm*Bgt17A with high transglycosylation ability.

The catalytic mode of *Rm*Bgt17A consists of a retaining reaction in which a general acid/base catalyst (proton donor, Glu99) acts first as an acid and then as a base in two steps: glycosylation and deglycosylation (Fig. 6*c*). In the first step, a $\beta$-1,3-glucan occupies binding sites −3 to +2 and a proton donor (Glu99) facilitates the departure of the leaving group by donating a proton to the O atom between the glycosyl moieties at sites −1 and +1, while the nucleophile (Glu189) forms an enzyme-sequestered covalent intermediate with the $\beta$-1,3-glucan residue. For the unique catalytic cleft of *Rm*Bgt17A, the leaving group can only be a laminaribiose. In the second step, a polysaccharide or oligosaccharide occupies binding sites +1 and +2 as an acceptor; the deprotonated proton donor (Glu99) acts as a general base to activate the C6 hydroxyl of the acceptor, which then carries out a nucleophilic attack on the $\beta$-1,3-glucan glycosyl-enzyme intermediate, leading to the formation of a new transglycosylation product, which adopts a $\beta$-1,6 linkage to the reducing end of $\beta$-1,3-glucan glycosyl. The three key residues (Tyr102, Trp157 and Glu158) in binding sites +1 and +2 can stabilize the transglycosylation transition and lead the reaction towards transglycosylation but not hydrolysis.

## 4. Conclusion

In this study, a GH family 17 $\beta$-1,3-glucanosyltransferase from *R. miehei* (*Rm*Bgt17A) and its inactive mutant E189A in

complex with laminaribiose and laminaripentaose were structurally characterized at resolutions of 1.30, 2.27 and 2.30 Å, respectively. *Rm*Bgt17A adopted the classical $(\beta/\alpha)_8$ TIM-barrel architecture, similar to the other enzymes in GH family 17. However, structural superposition of *Rm*Bgt17A on other reported GH family 17 enzymes demonstrated that *Rm*Bgt17A lacks the subdomain around helix $\alpha$6 at the end of the catalytic cleft. In addition, four surface residues (Tyr135, Tyr136, Glu158 and His172) were found near the reducing terminus of the +2 glycosyl site, blocking the catalytic cleft. The most prominent structural feature of *Rm*Bgt17A was a shorter catalytic cleft than in all other known GH family 17 enzymes. This unique catalytic cleft can only provide five subsites (−3, −2, −1, +1 and +2). Site-directed mutagenesis studies suggested that the excellent transglycosylation ability of *Rm*Bgt17A might be owing to stabilizing interactions within the acceptor and the catalytic cleft in subsites −1, +1 and +2. The structural features of *Rm*Bgt17A explain the biochemical properties of GH family 17 $\beta$-1,3-glucanosyltransferases, which cleave a laminaribiose from the reducing end of linear $\beta$-1,3 glucans.

## Acknowledgements

This work was supported in part by the National Science Fund for Distinguished Young Scholars (No. 31325021), the Program for Chang Jiang Scholars (No. T2014055) and the German Fellowship Programme for S&T Awardees. We are grateful to the staff of the SSRF and BSRF for their assistance in X-ray data collection.

## References

Adams, P. D. *et al.* (2010). *Acta Cryst.* D**66**, 213–221.
Afonine, P. V., Grosse-Kunstleve, R. W., Echols, N., Headd, J. J., Moriarty, N. W., Mustyakimov, M., Terwilliger, T. C., Urzhumtsev, A., Zwart, P. H. & Adams, P. D. (2012). *Acta Cryst.* D**68**, 352–367.
Chen, L., Garrett, T. P. J., Fincher, G. B. & Hoj, P. B. (1995). *J. Biol. Chem.* **270**, 8093–8101.
Chen, V. B., Arendall, W. B., Headd, J. J., Keedy, D. A., Immormino, R. M., Kapral, G. J., Murray, L. W., Richardson, J. S. & Richardson, D. C. (2010). *Acta Cryst.* D**66**, 12–21.
Davies, G. & Henrissat, B. (1995). *Structure*, **3**, 853–859.
Douglas, C. M. (2001). *Med. Mycol.* **39**, 55–66.
Emsley, P., Lohkamp, B., Scott, W. G. & Cowtan, K. (2010). *Acta Cryst.* D**66**, 486–501.
Fibriansah, G., Masuda, S., Koizumi, N., Nakamura, S. & Kumasaka, T. (2007). *Proteins*, **69**, 683–690.
Fontaine, T., Simenel, C., Dubreucq, G., Adam, O., Delepierre, M., Lemoine, J., Vorgias, C. E., Diaquin, M. & Latgé, J.-P. (2000). *J. Biol. Chem.* **275**, 27594–27607.
Gastebois, A., Mouyna, I., Simenel, C., Clavaud, C., Coddeville, B., Delepierre, M., Latge, J.-P. & Fontaine, T. (2010). *J. Biol. Chem.* **285**, 2386–2396.
Goldman, R. C., Sullivan, P. A., Zakula, D. & Capobianco, J. O. (1995). *Eur. J. Biochem.* **227**, 372–378.
Hartland, R. P., Emerson, G. W. & Sullivan, P. A. (1991). *Proc. R. Soc. B Biol. Sci.* **246**, 155–160.
Holm, L. & Rosenström, P. (2010). *Nucleic Acids Res.* **38**, W545–W549.
Hreggvidsson, G. O., Dobruchowska, J. M., Fridjonsson, O. H., Jonsson, J. O., Gerwig, G. J., Aevarsson, A., Kristjansson, J. K., Curti, D., Redgwell, R. R., Hansen, C. E., Kamerling, J. P. & Debeche-Boukhit, T. (2011). *Glycobiology*, **21**, 304–328.
Hurtado-Guerrero, R., Schüttelkopf, A. W., Mouyna, I., Ibrahim, A. F., Shepherd, S., Fontaine, T., Latgé, J.-P. & van Aalten, D. M. F. (2009). *J. Biol. Chem.* **284**, 8461–8469.
Kabsch, W. & Sander, C. (1983). *Biopolymers*, **22**, 2577–2637.
Klebl, F. & Tanner, W. (1989). *J. Bacteriol.* **171**, 6259–6264.
Kleywegt, G. J. (1999). *Acta Cryst.* D**55**, 1878–1884.
Lombard, V., Golaconda Ramulu, H., Drula, E., Coutinho, P. M. & Henrissat, B. (2014). *Nucleic Acids Res.* **42**, D490–D495.
Manners, D. J., Masson, A. J. & Patterson, J. C. (1973). *Biochem. J.* **135**, 19–30.
McCoy, A. J., Grosse-Kunstleve, R. W., Adams, P. D., Winn, M. D., Storoni, L. C. & Read, R. J. (2007). *J. Appl. Cryst.* **40**, 658–674.
McWilliam, H., Li, W., Uludag, M., Squizzato, S., Park, Y. M., Buso, N., Cowley, A. P. & Lopez, R. (2013). *Nucleic Acids Res.* **41**, W597–W600.
Mouyna, I., Fontaine, T., Vai, M., Monod, M., Fonzi, W. A., Diaquin, M., Popolo, L., Hartland, R. P. & Latgé, J.-P. (2000). *J. Biol. Chem.* **275**, 14882–14889.
Mouyna, I., Hartl, L. & Latge, J.-P. (2013). *Front. Microbiol.* **4**, 81.
Mouyna, I., Hartland, R. P., Fontaine, T., Diaquin, M., Simenel, C., Delepierre, M., Henrissat, B. & Latgé, J.-P. (1998). *Microbiology*, **144**, 3171–3180.
Müller, J. J., Thomsen, K. K. & Heinemann, U. (1998). *J. Biol. Chem.* **273**, 3438–3446.
Murshudov, G. N., Skubák, P., Lebedev, A. A., Pannu, N. S., Steiner, R. A., Nicholls, R. A., Winn, M. D., Long, F. & Vagin, A. A. (2011). *Acta Cryst.* D**67**, 355–367.
Otwinowski, Z. & Minor, W. (1997). *Methods Enzymol.* **276**, 307–326.
Receveur-Bréchot, V., Czjzek, M., Barre, A., Roussel, A., Peumans, W. J., Van Damme, E. J. & Rougé, P. (2006). *Proteins*, **63**, 235–242.
Robert, X. & Gouet, P. (2014). *Nucleic Acids Res.* **42**, W320–W324.
Rodríguez-Romero, A., Hernández-Santoyo, A., Fuentes-Silva, D., Palomares, L. A., Muñoz-Cruz, S., Yépez-Mulia, L. & Orozco-Martínez, S. (2014). *Acta Cryst.* D**70**, 329–341.
Sarthy, A. V., McGonigal, T., Coen, M., Frost, D. J., Meulbroek, J. A. & Goldman, R. C. (1997). *Microbiology*, **143**, 367–376.
Sestak, S., Hagen, I., Tanner, W. & Strahl, S. (2004). *Microbiology*, **150**, 3197–3208.
Street, I. P., Kempton, J. B. & Withers, S. G. (1992). *Biochemistry*, **31**, 9970–9978.
Tang, Y., Yang, S., Yan, Q., Zhou, P., Cui, J. & Jiang, Z. (2012). *J. Agric. Food Chem.* **60**, 2354–2361.
Terwilliger, T. C. & Berendzen, J. (1999). *Acta Cryst.* D**55**, 501–505.
Teze, D., Hendrickx, J., Czjzek, M., Ropartz, D., Sanejouand, Y.-H., Tran, V., Tellier, C. & Dion, M. (2014). *Protein Eng. Des. Sel.* **27**, 13–19.
Varghese, J. N., Garrett, T. P. J., Colman, P. M., Chen, L., Høj, P. B. & Fincher, G. B. (1994). *Proc. Natl Acad. Sci. USA*, **91**, 2785–2789.
Verdonk, M. L., Cole, J. C., Hartshorn, M. J., Murray, C. W. & Taylor, R. D. (2003). *Proteins*, **52**, 609–623.
Wessels, J. G. H. (1988). *Acta Bot. Neerl.* **37**, 3–16.
Wojtkowiak, A., Witek, K., Hennig, J. & Jaskolski, M. (2012). *Acta Cryst.* D**68**, 713–723.
Wojtkowiak, A., Witek, K., Hennig, J. & Jaskolski, M. (2013). *Acta Cryst.* D**69**, 52–62.
Zhou, P., Zhang, G., Chen, S., Jiang, Z., Tang, Y., Henrissat, B., Yan, Q., Yang, S., Chen, C.-F., Zhang, B. & Du, Z. (2014). *BMC Genomics*, **15**, 294–307.